Experimental and Numerical Analyses of a Novel Wing-in-Ground Vehicle

van Sluis, M.; Nasrollahi, S.; Gangoli Rao, A.; Eitelberg, G.

DOI
10.3390/en15041497

Publication date
2022

Document Version
Final published version

Published in
Energies

energies

MDPI

Article

Experimental and Numerical Analyses of a Novel Wing-in-Ground Vehicle

Martijn van Sluis *, Sina Nasrollahi, Arvind Gangoli Rao and Georg Eitelberg

Faculty of Aerospace Engineering, Delft University of Technology, 2629 HS Delft, The Netherlands; sina.nasrollahi@outlook.com (S.N.); a.gangolirao@tudelft.nl (A.G.R.); g.eitelberg@tudelft.nl (G.E.)
* Correspondence: m.vansluis@tudelft.nl

Abstract: The AeroCity is a new form of transportation concept that has been developed to provide high-speed ground transportation at a much lower cost than the existing high-speed railway. Utilizing the Wing-in-Ground (WIG) effect, the AeroCity vehicle does not require complex infrastructures like other contemporary concepts, such as the Hyperloop or Maglev trains. In the current work, the aerodynamic characteristics of the AeroCity vehicle are examined through a Computational Fluid Dynamics (CFD) analysis. The results from the CFD analysis qualitatively match with the findings of wind tunnel experiments. Surface streamlines and boundary layer measurements correspond well with the numerical data. However, the force measurements show a discrepancy. It is found that the separation bubble over the side plates is not captured by the CFD, and this is responsible for an under-prediction of the drag at higher free-stream velocities. The Transition SST model improved the matching between the experiments and numerical simulations. The influence of the moving ground is numerically investigated, and the effect of non-moving ground on the vehicle aerodynamics was found not to be significant. Finally, the inclusion of the track wall is examined. It is found that the merging of the wingtip vortices is responsible for a significant drag increase and, therefore, an alternative track geometry should be investigated.

Keywords: AeroCity; ground effect; WIG; aerodynamics; CFD

Citation: Van Sluis, M.; Nasrollahi, S.; Gangoli Rao, A.; Eitelberg, G. Experimental and Numerical Analyses of a Novel Wing-in-Ground Vehicle. *Energies* **2022**, *15*, 1497. https://doi.org/10.3390/en15041497

Academic Editor: Joseph Katz

Received: 22 November 2021
Accepted: 8 February 2022
Published: 17 February 2022

Publisher's Note: MDPI stays neutral with regard to jurisdictional claims in published maps and institutional affiliations.

1. Introduction

In our modern day society, there is an ever-increasing need for faster means of transportation to connect cities and urbanized regions. Traditionally, high-speed railway systems, such as the TGV, have been employed to fulfil this task. However, the cost associated with the development of a new high-speed connection is exorbitantly high. For example, the development cost for the Dutch HSL project was estimated to be around EUR 11 billion. On average, the infrastructure cost per 100 km of high-speed track in Europe is estimated to be around EUR 3.4 billion [1]. This is more than double the cost compared to a conventional rail track. In the case of MAGLEV trains, the cost for the development of the infrastructure alone is even higher, and is estimated to be around EUR 8.0 billion per 100 km of track. Due to the high development cost, the expansion of the current high-speed rail network is difficult, since the available budgets from governments for large infrastructural projects are limited. With this in mind, the AeroCity concept was developed [2]. By utilizing the Wing-in-Ground (WIG) effect, AeroCity avoids the need for complex infrastructure, such as high-tolerance track or vacuum tubes, etc. As such, the cost for the development of the infrastructure is foreseen to be 30–40% lower compared to traditional high-speed rail. This cost saving can be achieved since the required infrastructure for AeroCity is less complex [2].

The AeroCity vehicle (shown in Figure 1) is aerodynamically shaped with a low aspect ratio wing, which is used both for the generation of the required lift force, as well as

for accommodating passengers. Side plates are attached to the wing to enhance aerodynamic efficiency. Despite the low aspect ratio, AeroCity can achieve similar lift-to-drag (L/D) compared to modern airliners. The vehicle weighs approximately 26 tons and is 20 m in length, 8 m wide and close to 4 m high. A retractable wheel system is located inside the side plates for taxiing near stations and low-speed operations. During the initial phases of the journey, AeroCity will accelerate to 160 km/h before lifting off from the track. When airborne, AeroCity will fly approximately 0.05 m from the track surface to fully exploit the Wing-in-Ground effect. During the cruise flight, AeroCity will reach flight speeds of well over 300 km/h. In terms of propulsion, AeroCity will be electrically driven, for example, by an electric podded fan, to allow for a net emission-free transportation system. Flaperons and rudders are employed to provide lateral and longitudinal stability, as well as providing a means to control the flight height of the vehicle. Depending on the seating configuration, AeroCity can accommodate 80–100 passengers.

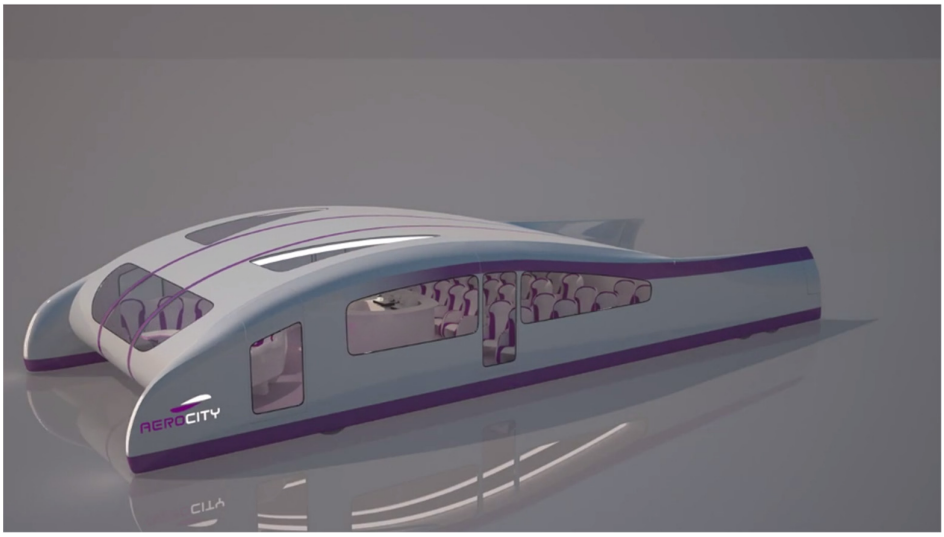

Figure 1. Artist rendering of the AeroCity, the Wing-in-Ground (WIG) effect vehicle. Courtesy of Movares B.V (Utrecht, The Netherlands).

The current work aims to gain further insight into the aerodynamic characteristics of AeroCity using experiments and CFD simulations. Previous work conducted on this topic includes a CFD sensitivity study [3] of the aerodynamic performance of AeroCity. Although this study has contributed to the knowledge about the aerodynamic characteristics of AeroCity, no verification or validation of the research findings have been provided. One of the main tasks of the current work is to perform numerical simulations, along with wind tunnel experiments, to understand the unique aerodynamic characteristics of this novel vehicle.

2. Literature

The Wing-in-Ground (WIG) effect has been known about since the early days of aviation. During landing, pilots experienced a 'cushioning of air' below the wing, which enhances the lift-to-drag ratio. WIG vehicles, such as the famous ekranoplan, were designed specifically to exploit this phenomenon to their benefit. The WIG effect entails multiple aerodynamic phenomena that alter the behaviour of a lifting surface in ground proximity. At a very low elevation above the ground, the viscous interaction of the flow with the ground plane plays a prominent role. To distinguish the various effects, they are categorized as chord-dominated and span-dominated effects. This distinction between two-dimensional and three-dimensional effects is helpful for the further analysis of WIG vehicles.

2.1. Chord-Dominated Effects

When an airfoil operates in close vicinity to the ground, the flow is affected due to the presence of the ground. In general, the location of the dividing streamline and the stagnation point are altered. When the flow channel between the airfoil and the ground plane is reduced, the pressure on the lower side of the airfoil is, in most cases, observed to increase. Ahmed [4] showed with wind tunnel experiments that, for a NACA 0015 symmetrical airfoil, a large portion of the incoming flow is directed over the upper surface as a result of flow deceleration on the pressure side of the airfoil, when the elevation is reduced. As a result of increased suction over the upper surface and pressure at the lower surface, the lift was found to increase. When reducing the elevation of the airfoil above the ground, the stagnation point was found to move in the downstream direction. As a consequence, the suction peak was enhanced. Due to the increased mean velocity of the upper surface, flow separation near the trailing edge was found to be postponed. Together with the observed increase in the lift, the lift-to-drag ratio of the airfoil was increased significantly due to the presence of the ground plane.

In a follow-on study, Ahmed [5] investigated the effect of camber on the aerodynamic performance of airfoils in close ground proximity. It was observed that, for a symmetrical airfoil at a low angle of attack, a convergent-divergent duct exists between the airfoil and the ground plane. Due to the Venturi effect, the pressure underneath the airfoil is locally reduced. As a consequence, the total lift generated by the airfoil was adversely affected. In combination with the higher local skin friction drag, the aerodynamic efficiency of the airfoil in ground proximity was decreased. For a NACA 4412, Ahmed [6] found that, at low ground clearances, the adverse pressure gradient in the flow channel underneath the vehicle is very high. As a consequence, laminar separation of the flow is observed downstream of the throat. To prevent the Venturi effect in close ground proximity, Ahmed [7] suggests the use of an airfoil with a position of maximum thickness relatively far aft, and a flattish lower surface at a small inclination at the design cruise angle of attack.

In a numerical analysis, Hsiun and Chen [8] showed that the aerodynamic performance of a NACA 4412 airfoil at low h/c, or height-to-chord ratio, is affected by the boundary layer of the stationary ground plane. Note that the Reynolds number in their analysis was relatively low, at $Re = 2.0 \times 10^5$. Although the lift coefficient initially increased with the reduction in elevation, a pronounced detrimental effect on the lift coefficient at the lowest h/c and free-stream velocity was observed. Hsiun and Chen conclude that this is due to the ground boundary layer, as the displacement thickness of the boundary layer reduced the effective height-to-chord ratio. As a result, the mass flux underneath the airfoil is reduced. Another discovery by Hsiun and Chen is the presence of a recirculation zone between the leading edge and the ground plane at $h/c = 0.05$ and at moderate values of α. According to Hsiun and Chen, this is 'because of the very small h/c value, the high angle of attack and the viscous effect'.

A better explanation for the recirculation zone is provided by Yang et al. [9] In a numerical study, Yang et al. showed that the ground boundary layer near the leading edge is subjected to a strong adverse pressure gradient. As a consequence, the displacement thickness of the ground boundary layer increases at a larger rate. If the adverse pressure gradient is sufficiently large, for example, due to a lower h/c, the ground boundary layer is prone to separation. As Yang et al. showed, the elevation of the airfoil with respect to the ground plane should be reduced with the displacement thickness of the ground boundary layer. In their specific case, the geometric $h/c = 0.10$ was reduced to an effective $h_e/c = 0.076$. As a consequence, the ground effect is over-predicted, as the apparent flight height is lower.

However, most of the studies mentioned above made use of a stationary ground boundary condition [4,5,7,8]. In a series of wind tunnel experiments on idealized ground–vehicle buff bodies, George [10] found that there is a significant difference in the lift and drag characteristics of the models between stationary and moving ground. The effect of the boundary condition was also investigated by Yang et al. [9], who investigated the use

of three different boundary conditions for the ground plane. This included a stationary ground, a moving ground and a symmetry boundary condition. Due to the absence of the ground boundary layer, no separation bubble is present for the latter two boundary conditions. Yang et al. conclude that the aerodynamic results obtained from an experiment using a fixed ground plane either over-predict or under-predict the ground effect, depending on if a separation bubble is present or not.

In a separate study, Barber [11] investigated the use of four different boundary conditions. In addition to the previously mentioned boundary conditions, a 'slip wall' condition was also incorporated. The latter implies that the shear stress at the wall is equal to zero. By using CFD analysis, the flow past a NACA 4412 at h/c = 0.025 was simulated for all four boundary conditions. As previously observed by Hsiun and Chen, a separation bubble was found to exist in the case of a stationary ground boundary condition. In the case of a moving wall or symmetry condition, flow reversal was not observed. A noticeable difference between the slip and moving wall boundary conditions is the velocity profile near the wall. In the case of the moving wall, the velocity is equal to the free-stream velocity. On the contrary, the velocity profile near a slip wall is almost constant and equal to the local velocity. Especially when the h/c is further reduced, the different velocity gradients near the wall will affect the aerodynamic performance of the wing significantly. A comparison of the lift-to-drag ratio for the different airfoils showed that only a stationary ground condition predicts a continuous increase in the L/D when h/c is reduced. The other models show a decrease when h/c < 0.05. The moving wall condition consistently predicted a lower L/D ratio compared to the other boundary conditions.

Together with the PIV measurements obtained from a low-speed wind tunnel experiment, Barber concludes that a moving ground boundary condition is the only physically correct representation of the ground for WIG effect studies. This is in agreement with the previous statements by George [8], who concluded that a moving wall boundary condition should be applied when h/c is reduced below h/c < 0.10.

Since the key factor for the WIG effect appears to be predominantly caused by an increase in the pressure underneath the wing, research has been conducted to further enhance the lower-side pressure. Ockfen and Matveev [12] investigated the use of a trailing edge flap to enhance lift generation. Utilizing a numerical study involving RANS, the use of either a split flap or a plain flap was investigated. Their effect on the aerodynamic performance of the airfoil was tested for various flap deflections. The flap deflection was defined as the vertical distance y_f, which was measured between the trailing edge of the airfoil and the flap. Furthermore, the distance h_f between the trailing edge of the flap and the ground plane was defined. A moving ground boundary condition was applied. The various configurations were tested at $\mathrm{Re} = 1.0 \times 10^6$ and for a range of $\alpha = 2° - 6°$ and h/c = 0.05–0.15. It was discovered that the deflection of a flap increased the lift in all cases. The deployment of the flap reduces the effective trailing edge height and, therefore, increases the pressure underneath the airfoil. In the limiting case ($h_f \to 0$), the full stagnation of the flow is obtained. However, the flow on the upper surface was observed to separate near the trailing edge for large flap deflections. In all cases, the flap deflection increased the total drag of the airfoil. This is primarily because the flap adds additional area perpendicular to the incoming flow. Moreover, the occurrence of flow separation over the upper surface also contributes to the overall larger drag. Ockfen and Matveev [12] found that a small flap deflection ($h_f/c = 0.025$) yielded the largest increase in the L/D ratio. In the case of flap deflections larger than ($h_f/c = 0.05$), the aerodynamic efficiency was reduced due to the relative increase in the pressure drag compared to the additional aerodynamic lift. Therefore, Ockfen and Matveev conclude that a small flap deflection, using either a plain or split flap, could be used to enhance the lift-to-drag ratio for WIG vehicles.

In order to enhance the fundamental understanding of the WIG effect, Hase et al. [13] employed the Thin Airfoil Theory to analyse the aerodynamic characteristics of airfoils in ground proximity. Based on a lumped vortex approach, it was shown that, for a front-loaded airfoil, the lift increases due to the presence of the ground plane. Based on these

expressions, a decrease in the lift is expected for an aft-loaded airfoil. To test if the simplified representation of the ground effect is valid, a wind tunnel experiment was conducted. For this purpose, a symmetric NACA 0012, a NACA 6212 and a NACA 6712 were tested. Note that the airfoils have identical thicknesses and camber, but only differ in the location of maximum camber. The experiment was conducted in the M-tunnel of the TU Delft, with the chord-based Reynolds number being around $Re = 1.8 \times 10^5$. Further, the model span was equal to b = 400 mm and AR = 4.4. To prevent interference with the wind tunnel walls, the ceiling of the tunnel was removed. Use was made of a stationary ground plane. Since the lowest elevation used for testing was h/c = 0.30, it was assumed that the influence of the ground boundary condition can be neglected.

The experimental data showed that, in the case of the NACA 6712, the ground proximity reduces the lift coefficient when normalized with the out-of-ground effect lift coefficient. The latter was assumed to be the case when h/c = 1.5. The front-loaded NACA 6212, on the other hand, showed a modest improvement of the lift coefficient when the elevation was reduced. In all cases, the effect of the ground plane appeared to be most favourable towards the higher-lift conditions. A comparison of the lift measurements with the predictions of the thin airfoil theory showed little agreement. This is explained by Hase et al., who claim that it is due to the exclusion of the thickness effect by the analytical expressions. In order to better understand the underlying aerodynamic principles, a series of PIV measurements were conducted, both for high- and low-lift conditions. Again, the results were compared with out-of-ground effect conditions. In the case of the lower-lift conditions (low angle of attack), the non-dimensionalized lift was found to decrease due to the occurrence of a convergent-divergent duct between the airfoil and the ground plane. Especially in the case of the NACA 6712, this resulted in a significant decrease in the pressure on the lower side of the airfoil. For a higher-lift condition, the Venturi effect was not present. In the case of the NACA 0012 and NACA 6212, the presence of the ground plane had a positive effect on the lift generation. For the aft-loaded NACA 6712, there was no beneficial effect of the ground proximity. Hence, in addition to the statements by Ahmed [5] concerning the location of maximum thickness, the study by Hase et al. shows the importance of the location of maximum camber for the aerodynamic performance of airfoils in the ground proximity.

The effect of camber is also acknowledged by Gross and Traub [14]. Using also a lumped vortex positioned at x = 1/4c, it was shown that, in the case of potential flow, two separate effects occur. First, a cambering effect, due to a change in up-wash by the vortex, was identified. Second, a reduction in the free-stream velocity was observed as a consequence of an upstream velocity component of the induced vortex flow. Gross and Traub developed a semi-empirical formulation to estimate the ground effect on airfoil performance, based on the airfoil coefficients obtained for the out-of-ground effect. To check the validity of the semi-empirical relation, a wind tunnel experiment was conducted for a S8036 profile. Testing was conducted at $Re = 1.8 \times 10^5$ in an open-return wind tunnel. To mimic the ground plane, an adjustable splitter plate was used. When comparing the experimental and analytical results for the out-of-ground effect, it was found that there is a good agreement. When the elevation was reduced, the deviation grew gradually. Note that the lowest elevation was limited to h/c = 0.1. Nevertheless, based on these findings, it can be concluded that the theoretical modelling of the ground effect might be a suitable tool for the initial prediction of airfoil behaviour in ground proximity.

2.2. Span-Dominated Effects

Already in the 1920s, Wieselberger [15] started to investigate the WIG effect. Using the wing theory by Prandtl [16] and the multi-plane theory developed by Betz [17], Wieselberger showed that the lift–drag polar of an airfoil in the proximity of a ground surface could be determined analytically, once the lift–drag polar out-of-ground effect is known. Since Wieselberger assumed an elliptical lift distribution, the formulation is not very useful for the analysis of the low aspect ratio wings typically found on WIG craft. In order to

address this, Philips and Hunsaker [18] derived a series of improved formulations, accounting for various wing platforms. Their study showed that the so-called influence factor is not only a function of the wing height-to-span (h/b) ratio, but is also influenced by the lift coefficient, planform and aspect ratio of the wing. Traub [19] used the expression for non-tapered wings created by Philips and Hunsaker [18] to develop an analytical approach for the development of WIG craft. In conjunction with the theoretical predictions, a series of wind tunnel experiments for sectional and finite wing models were performed. Using the 2D data as the input for the analytical model, Traub showed that the analytic predictions for the finite wing are in good agreement with the 3D wind tunnel results. Especially in the case of the lowest aspect ratio (AR = 3.46) wing, the results were promising. In the case of a higher aspect ratio (AR = 5.18), the deviation below h/c = 0.4 is more pronounced. In closer proximity to the ground, the deviation between the model and wind tunnel results grows for both wings. According to Traub, this is because the method created by Philips and Hunsaker translates a loss in leading edge suction into additional pressure drag. Close to the ground, an increase in leading edge suction is observed for the S8032 profile under consideration.

Due to practical limitations, the aspect ratio of a WIG craft is in general limited to low aspect ratio wings. To understand the influence of the aspect ratio for wings with extreme ground effects, Fink and Lastinger [20] performed a series of wind tunnel measurements on low aspect ratio wings. An image model was used to prevent viscous interaction with a ground plane. Furthermore, a modified Glenn Martin 21 airfoil was used, with a flattened lower surface to exclude the occurrence of the Venturi effect. Fink and Lastinger reported an increase in the lift curve slope and a reduction in the induced drag when the elevation was reduced. In line with expectations, the best aerodynamic efficiency was obtained for the wing with the highest aspect ratio at the lowest h/c. In comparison with the analytic predictions by Wieselberger [15], Fink and Lastinger obtained very similar results for the range h/b = 0.3 to h/b = 1.0. In closer proximity to the ground, the theoretical formulations again did not align with the experimental findings. This is in accordance with the observations made by Traub [19]. In order to enhance the aerodynamic performance of the lowest aspect ratio wing (AR = 1), the use of a wing side plate was investigated. By preventing high pressure air from 'escaping' around the wing tip, due to the presence of the side plate, a higher lift is maintained, while reducing the contribution of the induced drag. Indeed, it was found that the inclusion of side plates significantly improved the aerodynamic efficiency of the wing. Nevertheless, Fink and Lastinger note that an increase in the aspect ratio from AR = 1.0 to AR = 2.0 would still be more effective.

In a more condensed study, Chawla et al. [21] confirm the positive effect of side plates on the aerodynamic efficiency of low aspect ratio (AR = 2.33) Wing-in-Ground effect. Additionally, the use of a centre plate was investigated. However, this did not have any significant effect on the aerodynamic performance of the wing. In a more comprehensive numerical study, Park and Lee [22] examined the effect of side plates on a square wing using the modified Glenn Martin 21 airfoil. Using RANS, the CFD model was successfully validated with the findings of Fink and Lastinger [20]. For a more in-depth aerodynamic analysis, a moving ground boundary condition was applied. It was found that the side plates alter the behaviour of the trailing vortices. Two vortices are generated per side, including an upper and lower tip vortex. Although the vortex strength of the lower vortex was increased by the presence of the side plates, the aerodynamic efficiency was enhanced. In the case of side plates, the core of the lower vortex is displaced more in the lateral direction. As a consequence, the upper and lower vortices do not merge ahead of the trailing edge. Park and Lee conclude that a 'jet-like flow tends to push the wing-tip vortex at the lower surface. The distance between the two separated wing-tip vortices is too great to merge at the trailing edge'. Although it is suggested that this is beneficial for the overall drag production, no further analysis of the phenomenon was performed.

In a similar numerical experiment, Jung et al. [23] showed that the side plates significantly increase the pressure on the lower side of the wing. Again, it was noticed that the

tip vortex is displaced in the lateral direction in the case where side plates are installed. To better understand the behaviour of a trailing vortex sheet of a Wing-in-Ground effect, Cho and Han [24] examined the unsteady behaviour of a trailing vortex sheet in the proximity of the ground plane. The results were validated with the method proposed by Krasny [25]. Compared to a wing-out-of-ground effect, Cho and Han observed that the size of the vortex core is reduced when the ground is approached. Furthermore, the position of the vortex is found to shift in the lateral direction. Cho and Han further state that viscous interaction between the ground and the vortex could lead to separation of the ground boundary layer due to enhanced local cross-flow. When investigating the effect of flap deflection, it is observed that the presence of the ground prevents the flap and tip vortex from merging, despite having the same sense of rotation. Again, this results in two separate vortices, compared to a single vortex when in free flight.

Although the previous work shows that the use of side plates is beneficial, Park and Lee [22] discovered that the side plates have a negative effect on the longitudinal stability in the case of a square NACA 4412 wing. Only for a specific range of α was the Height Stability (H.S.) criterion met. However, this region did not coincide with the angle of attack for which the L/D is at maximum. Depending on the airfoil geometry and the design lift coefficient, this could limit the design space. As an alternative for side plates, Lee et al. [26] investigated the use of wing anhedral for enhancing the L/D ratio of wings for WIG craft. Using CFD, three configurations were investigated: a plain wing, a wing with side plates and a wing with an anhedral angle. In the case of a wing with side plates, the gap height between the ground and the side plate was kept constant at all times. Lee et al. found that the plain wing and the wing with side plates did not satisfy the H.S. criterion for certain values of α. However, the wing with anhedral did comply with the H.S. criterion for all angles of attack. According to Lee et al., this is mainly due to a shift of the neutral point with respect to elevation X_h. In terms of aerodynamic efficiency, the anhedral angle only improved the L/D ratio by a small margin compared to the plain wing. Therefore, Lee et al. recommend the combined use of an anhedral angle and side plates to enhance both the aerodynamic efficiency and stability of WIG craft.

3. Description of the Wind Tunnel Experiment

To verify the aerodynamic configuration, a series of wind tunnel experiments were performed on a basic aerodynamic model of the AeroCity vehicle. The main goal was to obtain a trustworthy experimental data set to be used for the future validation of follow-on CFD simulations

3.1. Wind Tunnel

Tests were conducted in the Low-Turbulence Tunnel (LTT) wind tunnel of the TU Delft. The LTT is driven by a six-bladed fan powered by a 525 kW DC motor. Due to a contraction ratio of 17.8, the turbulence intensity of the free stream is very low, measuring 0.015% at 20 m/s to 0.07% at 75 m/s. The test section is octagonal and measures 1.80 m × 1.25 m × 2.60 m (W × H × L). The test section is equipped with a mechanically actuated turntable, which is flush with the upper and lower walls. Using a six-component balance, the forces and moments on the model are measured. Data storage is provided by an electronic data acquisition system and lab computer. The maximum velocity at the test section is 120 m/s. For the current tests, the free-stream velocity was varied between 10 m/s and 100 m/s.

3.2. Model

A scaled model of the AeroCity concept (1:20), shown in Figure 2, was used for the wind tunnel analysis of the AeroCity concept. The chord length is 1020 mm, and the model span is 400 mm. The model has been constructed from SikaBlock M650 polyurethane foam and a CNC milling machine was used to translate the CAD model into a physical model.

The model consists of the main body with two side plates attached, each at one side. The side plates are attached by means of four M4 bolts per plate. The model itself was attached to the balance of the test section by a total of four M8 bolts. After construction, the model was sanded to obtain the desired surface roughness.

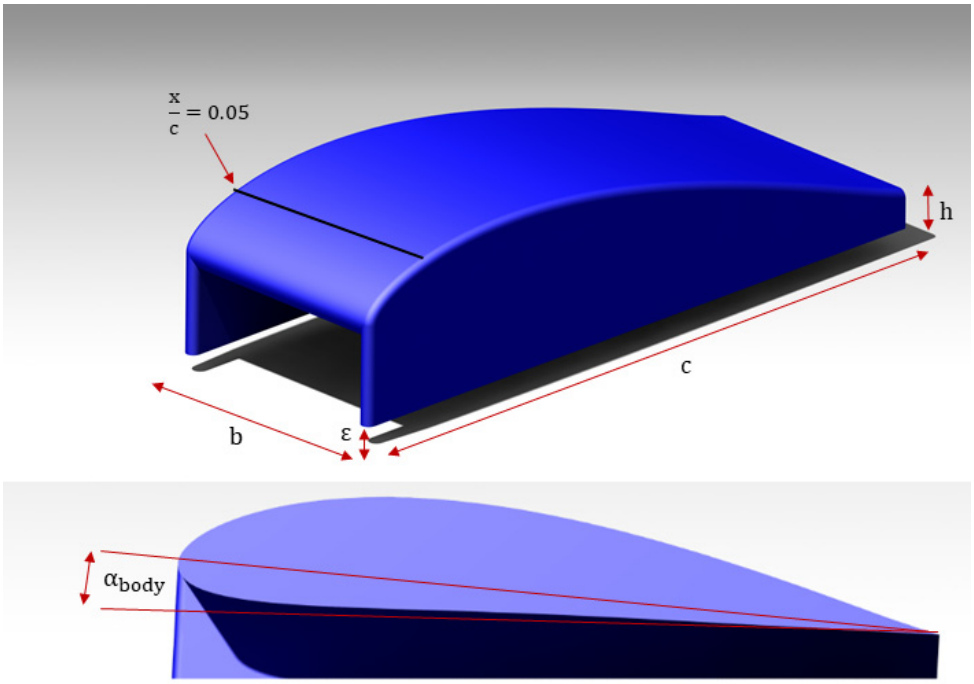

Figure 2. Basic aerodynamic shape of the AeroCity wind tunnel model. The most important design parameters are indicated.

The geometry of the main body consists of a NACA 68015 airfoil with a reflexed (S-shape) camber line. The width of the main body is equal to 350 mm. The attached side plates each have a width of 25 mm. The side plates are straight, except for the rounded outer edge (R = 12.5 mm) at the front of the side plate. The body's angle of attack and elevation were controlled by trimming the lower part of the side plates to match the specifications. The gap height between the side plate and the ground surface was controlled by employing spacers on the M8 bolts. To control the location of transition to turbulent flow, two adjacent layers of double-sided tape (thickness 0.25 mm) were used at x/c = 0.05. Utilizing a microphone, it was made sure that the flow was, indeed, turbulent downstream of the transition location.

3.3. Experimental Setup

During the experiment, several configurations have been used for wind tunnel testing. The main parameters that were studied are the body angle-of-attack, side plate elevation ε and relative body elevation h/c. In total, six different settings have been tested for one model configuration. For each setting, both a natural and a forced transition measurement were performed. The body's angle of attack was varied to be either 3 deg or 5 deg, while the relative body elevation was selected to be either h/c = 0.10 or h/c = 0.05. Finally, the gap height of the side plate was varied between 7 mm ($\varepsilon/h = 0.14$) and 3 mm ($\varepsilon/h = 0.06$). An overview of the various settings is presented in Table 1.

Table 1. Overview of the settings used for wind tunnel analysis.

#	α_{body}	h/c	ε
1	3 deg	0.10	3 mm
2	3 deg	0.05	7 mm
3	5 deg	0.10	3 mm
4	5 deg	0.10	7 mm
5	5 deg	0.05	3 mm
6	5 deg	0.05	7 mm

The model was mounted directly onto the balance scale on the ceiling of the wind tunnel test section, as shown in Figure 3. By using a relatively large-scale model, the influence of the wind tunnel boundary layer over the wind tunnel wall on the model was assumed to be limited. No efforts were made to suppress or eliminate the boundary layer over the wind tunnel wall. Force and moment measurements were obtained directly from the readings of the six-way balance. As the model was not equipped with pressure ports, pressure measurements were obtained from Pitot tube samples taken across the surface of the model. Only measurements from the upper surface and exterior surface of the side plates have been recorded. The procedure was as follows: the Pitot tube was mounted on the surface using a layered tape and connected to a digital pressure gauge. Depending on the local curvature of the body, the needle was elevated between 4 mm and 10 mm above the surface. After each measurement, the Pitot tube was removed and positioned at the next sampling location. Aside from static pressure samples, measurements of the total pressure along the surface were recorded. The latter was performed in order to map the development of the boundary layer over the upper surface and side plates of the AeroCity model. The procedure for this is slightly different. The Pitot tube was aligned with the local flow and gradually moved away from the surface after each sample. In order to increase the resolution of the findings, an average of the pressure readings over a period of 3 s (100 samples) was taken. The recording of the boundary layer properties was conducted at a free-stream velocity of 65 m/s. No corrections for, e.g., model blockage, were applied to the measurements. The cross-section area ratio of the model and the wind tunnel test section is 0.0367, based on a test section cross-section area of 2.07 m^2.

Figure 3. The AeroCity wind tunnel model suspended upside down in the test section of the Low-Turbulence Tunnel (LTT).

3.4. Results

A major part of the wind tunnel experiment was concerned with the acquisition of force and balance measurements for the various configurations. The trends of the lift coefficient with the free-stream velocity for both settings of the side plate gap height are shown in Figures 4 and 5. Similar to the observations by Nouwens [3], the lift increased significantly when the gap height was reduced. In terms of drag coefficient, the reduced gap height also has a positive influence on reducing drag. Overall, the difference amounted to almost 10% of the total vehicle drag. Note that, especially at the lower Reynolds numbers, the influence of the transition point is noticeable. However, the influence of the transition point is less obvious for the recorded lift coefficients. Only setting #3 (α = 5°, h/c = 0.10 and ε = 3 mm) appears to experience a significant difference in the lift, in the case that the upper surface boundary layer is not tripped at x/c = 0.05.

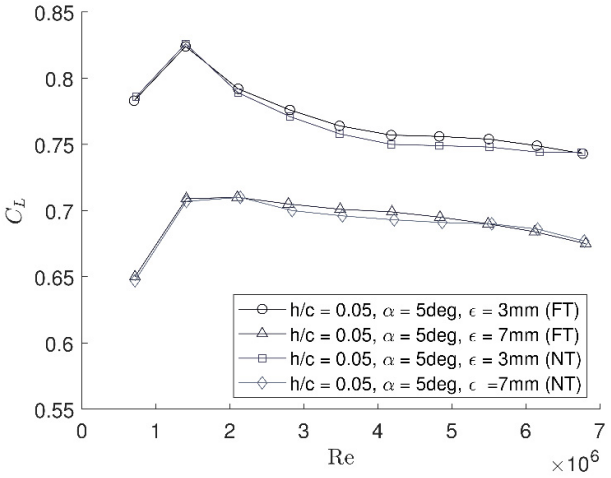

Figure 4. Variation in lift coefficient wit Re for two settings of the side plate gap height at h/c = 0.05. FT= Fixed Transition, NT = Natural Transition.

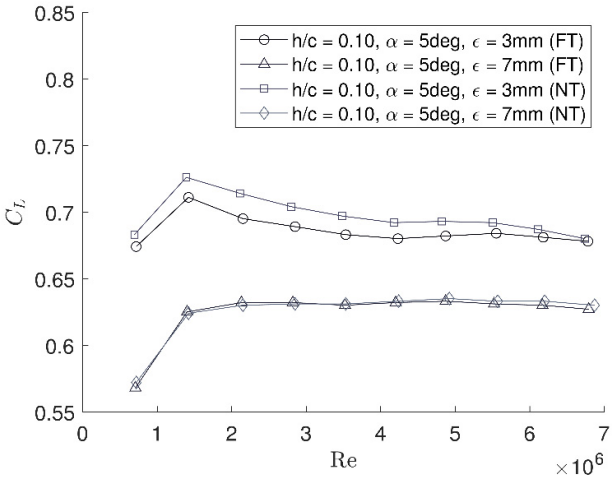

Figure 5. Variation in lift coefficient with Re for two settings of the side plate gap height at h/c = 0.10. FT= Fixed Transition, NT = Natural Transition.

A comparison of Figures 4 and 5 also shows the influence of the body elevation on the lift coefficient. Unlike Nouwens [3], both the elevation and the body's angle of attack measurements are taken around the trailing edge. As such, their individual contribution

can de distinguished. The influence of the body elevation is roughly equal to the influence of the side plate gap for the current model. Besides the investigation into the effect of the height parameters, the influence of the body's angle of attack was also explored. The difference in the lift coefficient for two incidence settings of the wing is shown in Figure 6. Apart from the obvious observations, such as an increase in both the lift and drag coefficient towards higher values for α, no distinct changes are observed between the two configurations. The same holds for the plot of the drag coefficient, shown in Figure 7.

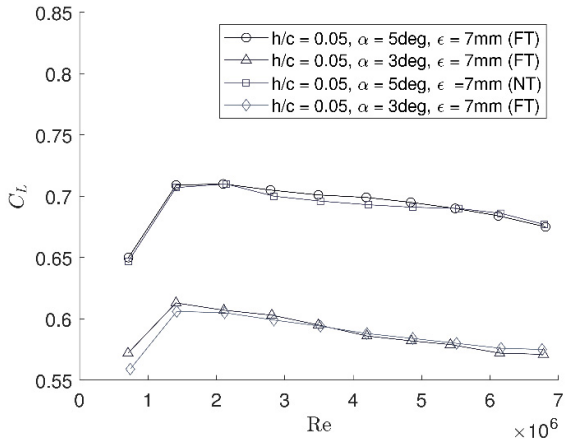

Figure 6. Comparison of lift for two settings of the body's angle of attack at identical height parameters. FT= Fixed Transition, NT = Natural Transition.

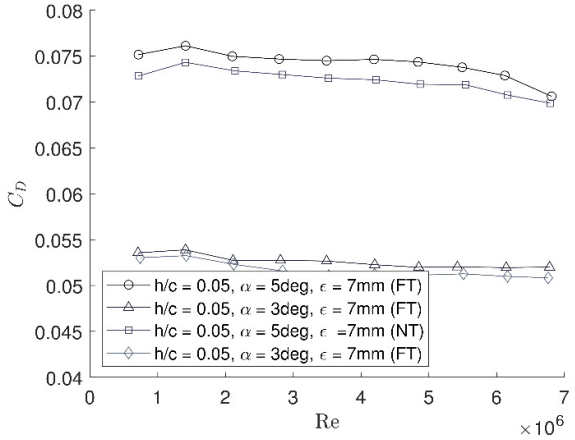

Figure 7. Comparison of the drag coefficient for two settings of the body's angle of attack at similar height. FT= Fixed Transition, NT = Natural Transition.

4. Numerical Simulation

In order to gain more insight into the aerodynamic characteristics of the AeroCity wind tunnel model, the numerical analysis of AeroCity was performed by using Computational Fluid Dynamics (CFD). Since the experimental data of the pressure distribution and the development of the vehicle upper boundary layer are available for $\alpha = 3°$, h/c = 0.05 and $\varepsilon = 7$ mm, this condition was selected for further study.

4.1. Numerical Methods

The flow around the wind tunnel model was assumed to be incompressible. The free-stream velocity in the numerical model was limited to 80 m/s to maintain the assumption

of flow incompressibility. This corresponds to a chord-based Reynolds number of Re = 5.6 × 10^6. The Reynolds Averaged Navier–Stokes (RANS) equations were selected to resolve the flow. ANSYS Fluent (Version 16.1), a commercial software package, was used to perform the numerical calculations. The ambient conditions were set equal to the conditions during the wind tunnel experiment. A velocity inlet boundary condition was applied at the inlet (5c upstream), and a pressure outlet (8c downstream) was selected to terminate the computational domain. The octagonal cross-section of the wind tunnel test section was simplified to a rectangular cross-section of identical dimensions. A schematic of the computational domain is shown in Figure 8. The pressure-based SIMPLEC [27] algorithm was selected to solve the pressure-velocity coupling. A third-order MUSCL [28] scheme was invoked for the discretization of the momentum equations. Turbulence properties were handled by the QUICK [29] scheme, and a staggered grid was used for the spatial discretization of the pressure field. The computations were performed on a dual CPU (12-core) HP Z-600 workstation, with 48 GB memory in total. Since the model is axisymmetric, only half of the model was used for CFD analysis.

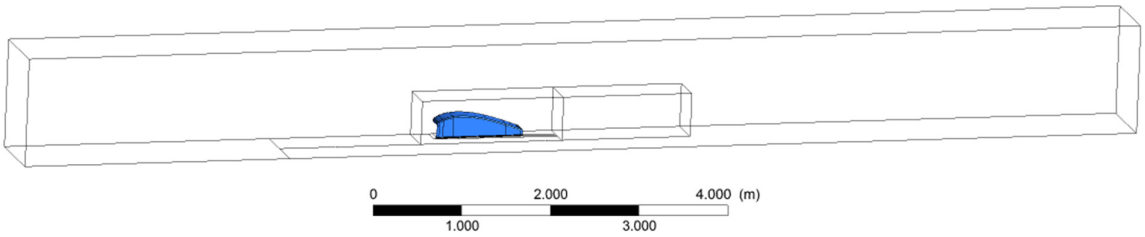

Figure 8. Schematic drawing of the computational domain. Shown are the AeroCity half-model, the rectangular body of influence and the division of the ground wall.

4.2. Validation

To improve the quality of the numerical results, considerable attention was paid to the setup and implementation of the numerical models. To select the most suited models and methods, a WIG study by Kumar [30] was selected as a validation case. Involving a medium-thickness wing equipped with side plates, the model configuration is similar to the basic aerodynamic model of AeroCity. Different from the AeroCity case is the use of a symmetric model to mimic the presence of the ground plane, rather than the use of a stationary wall. A photograph of the test setup is shown in Figure 9. Shown is the wing and the image model, suspended on struts. Note that the gap, which was reported to be 0.5 mm, is negligible compared to the model size (4 × 2 ft). Since it was assumed that the amount of leak flow through the gap is negligible, the gap height was ignored for the numerical simulation. The airfoil section used in the experiment is a Clark Y section, with a thickness-to-chord ratio of t/c = 11.7%. Even though this section is thinner than the AeroCity airfoil (t/c = 15%), the aerodynamic characteristics are similar. Testing was conducted in the low-turbulence wind tunnel of Cranfield University. The test section measures 2.4 m by 1.6 m, and is a closed section. The flow speed was set equal to 100 ft/s, which equates to a chord-based Reynold number of Re = 1.3 million. Wind-tunnel correction factors were applied to account for the blockage effects of the wing, struts and wake. The data for the lowest elevation height h/c = 0.084 and $\alpha = 2°$ have been selected for comparison. Note that the elevation height is measured with respect to the quarter-chord point.

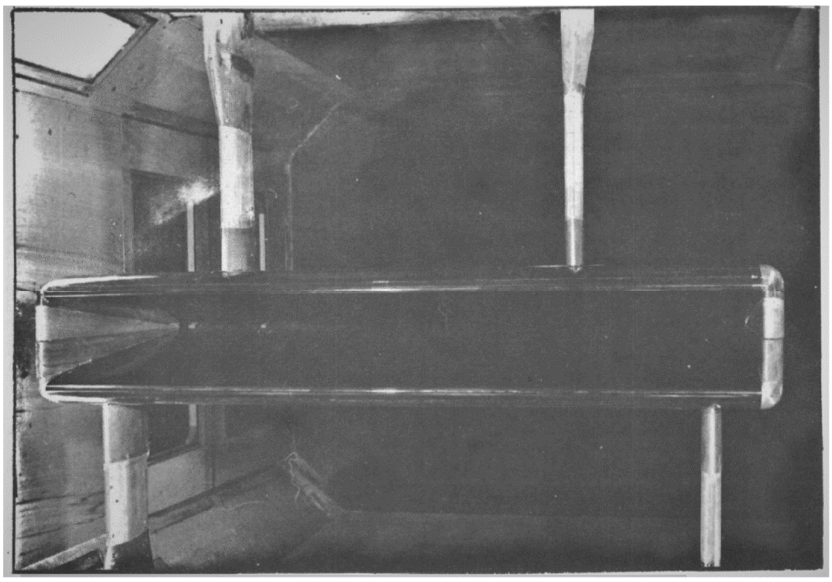

Figure 9. Photograph of the wind tunnel setup featuring the wing with half-airfoil endplates [30].

The computational domain represented the wind tunnel cross-section and extended 5c upstream and 8c downstream. A limited mesh convergence study was carried to determine the effect of the mesh cell size on the force predictions. By a subsequent mesh refinement of the fully unstructured tetrahedral mesh on the surface from $\Delta/c = 0.01184$ to $\Delta/c = 0.00492$, the number of cells was gradually increased. The Shear Stress Transport (SST) k-ω model was selected as a turbulence model, with $Y^+ \approx 1$ for the first-layer height of the wall-adjacent cells. The number of inflation layers was kept constant. As can be seen from Table 2, beyond 13.8 million cells, the relative improvement of the force predictions diminishes.

Table 2. Mesh dependency study for four different mesh sizes. Data compared with experimental data by Kumar [30].

Cells	C_L	Δ%	C_D	Δ%
4.7×10^6	0.5937	+6.59	0.00922	−16.94
13.8×10^6	0.5783	+3.82	0.00990	−10.86
18.6×10^6	0.5767	+3.53	0.00989	−10.80
27.5×10^6	0.5764	+3.48	0.00993	−10.54

To determine the influence of the turbulence model on the numerical results, two additional turbulence models were tested in combination with the 13.8 million-cell mesh. The results are shown in Table 3. The Spalart–Allmaras model appears to be better at predicting drag. However, in terms of lift coefficient, the accuracy is lower compared to the SST model. In contrast, the RSM model is close in terms of lift prediction, but shows a larger discrepancy in the predicted drag coefficient. The cause for the over-prediction of the aerodynamic efficiency by the numerical models, compared to the wind tunnel observations, is unclear. Possibly, the interaction of the flow between the struts and the model had a non-negligible effect on the force measurements. The model supports were not considered in the CFD analysis. Without a clear advantage of any turbulence model, the SST k-omega model is selected for further analysis.

Table 3. Comparison of CFD predictions with experimental data from Kumar [30], using different turbulence models. SST = Shear Stress Transport k-omega, SA = Spalart–Almaras and RSM = Reynolds Stress Model (k-omega based).

Turb Model	C_L	Δ%	C_D	Δ%
SST	0.5783	+3.82	0.00990	−10.54
SA	0.5808	+4.29	0.01020	−8.09
RSM	0.5658	+1.59	0.00933	−15.92

4.3. Grid

The computational domain was meshed utilizing an unstructured, tetrahedral-dominated mesh. Prism layers were applied to the ground-plane (wind tunnel roof) and the body of the wind tunnel model. In order to make sure that the boundary layers are resolved with sufficient accuracy, the wall-adjacent prism cells were refined such that $Y^+ \approx 1$. Since the available computational resources were limited, a prism layer growth ratio of r = 1.30 was selected. In total, 24 prism layers were applied. A rectangular body of influence was added to control the refinement of the volume mesh surrounding the model. A limited mesh dependency study was carried out to optimize the trade-off between computational load and numerical accuracy. It was found that the numerical results were most sensitive to changes in the volume mesh directly surrounding the model. Shown in Table 4 are the sensitivities of the model force coefficients with respect to the mesh total cell size. The coefficients are presented as relative deviations from the experimental results. Beyond 10 million elements, further refinement of the mesh does not appear to improve the lift force coefficient prediction significantly ($\Delta C_L \approx 0.25\%$). In terms of drag force prediction, the sensitivity to the mesh refinement is slightly more pronounced, with a relative change of $\Delta C_D \approx 0.50\%$. To balance the computational load, the medium-refinement mesh of 10 million elements was selected for further analysis. A close-up of the mesh around the AeroCity model is presented in Figure 10.

Table 4. Mesh dependency study for three different mesh sizes. Force coefficients are compared to the experimental data.

Cells	C_L	Δ%	C_D	Δ%
3.5×10^6	0.6158	−2.12	0.04623	+12.44
9.8×10^6	0.6022	+0.13	0.04730	+10.42
14.5×10^6	0.6007	+0.39	0.04762	+9.80

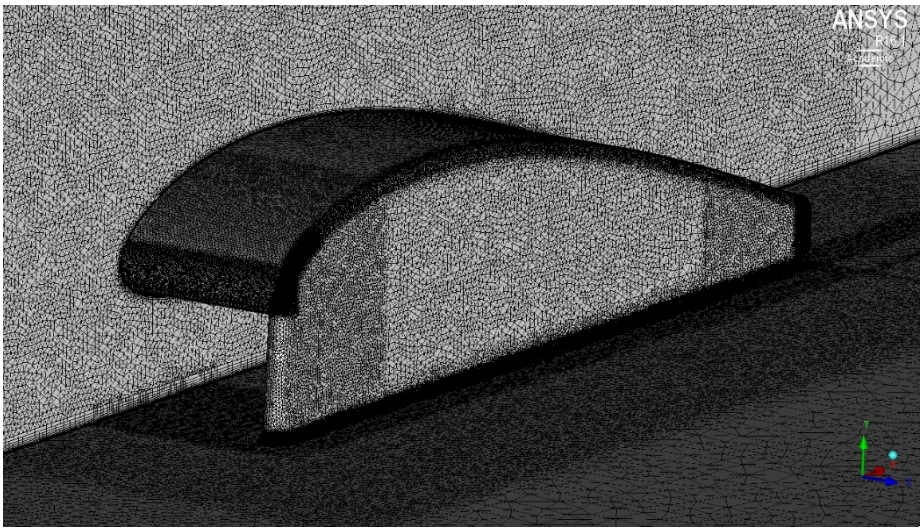

Figure 10. Close-up of the mesh constructed around the AeroCity model. Visible are the refinements of the mesh near the body and the prism layers over the ground plan. Additionally shown: the symmetry plane to reduce the computational load.

It should be noted that the development of the boundary layer over the wind tunnel wall was not measured during the experiments. However, a calibration measurement of the wall boundary layer of the empty tunnel was available. Using standard theory for a flat plate with a zero-pressure gradient, the virtual origin of the boundary layer was found through a comparison of the predicted displacement thicknesses. As such, the upstream ground surface was divided into a slip wall and a non-slip wall to control the onset of boundary layer growth. Successive CFD analysis, with the wind tunnel model removed from the computational domain, confirmed that the displacement thickness of the simulated boundary layer was on par with the experimental findings.

4.4. Numerical Results

The first step was to analyse the predicted force coefficients of the AeroCity model and compare these to the wind tunnel data. Shown in Figure 11 are the lift and drag coefficients measured over the range of free-stream velocities. As one can observe, the result in the lower velocity range (U < 40 m/s) are similar. Nevertheless, towards the higher free-stream velocity, the deviation between the experiment and simulation data grows considerably. At the highest velocity used for analysis, the deviation in the lift-to-drag ratio exceeds ΔL/D = 25%. Considering that the aerodynamic performance of the AeroCity at high speed is of most interest, the current deviation between the two data sets is troublesome. For the largest part, the deviation in L/D is due to an under-prediction in the drag coefficient, as the error for the lift coefficient is within a reasonable margin. If one compares the pressure distribution along the centre chord, it is found that the pressure distribution over the upper surface is almost identical. Nevertheless, two remarks can be made about the comparison of C_p, shown in Figure 12. First, a small jump in the pressure can be observed around x/c = 0.35. Although this may appear to be caused by a small separation bubble, it is believed to be a measurement error. As discussed earlier, the height of the Pitot tube above the surface was varied depending on the local curvature of the body. Since the shape of the upper surface transitions from concave to convex at x/c = 0.35, the height above the surface varied around this point. A second observation, made from Figure 12, is a small discrepancy of the C_p data towards the trailing edge. This may be an indication that, during the wind tunnel experiment, the boundary layer development was different in comparison with the predictions by the CFD model. However, without any other available data, a definitive conclusion cannot be provided at this point. Since the force coefficients showed a strong dependence on the free-stream velocity, the pressure distributions at various levels of free-stream velocity were examined. However, the C_p distributions remained identical, regardless of the free-stream velocity. Similarly, the pressure profile along the span was investigated. At half semi-span, the influence of the tip vortices was starting to become noticeable. The suction levels near the leading edge were reduced, while towards the trailing edge, slightly enhanced levels of C_P were observed. Further outboard, at the three-quarter semi-span, the effect of the tip vortex is pronounced. Significantly, near the trailing edge, the pressure distribution was affected strongly. Nevertheless, the pressure profiles at these span-wise stations were not altered by either decreasing or increasing the velocity of the free-stream. The comparison of the pressure contours at U = 40 m/s and U = 80 m/s, taken over the side plate of the AeroCity, shows that the pressure levels are significantly altered only near the leading edge of the side plates. At the higher free-stream velocity, the zone of low pressure in the vicinity of the side plate's leading edge is reduced. Hence, the area of separated flow is reduced at higher velocities. During the experiments, the existence of a separation bubble over the side plate was already observed. Therefore, it appears that the size of the separation bubble reduces when the velocity in the test section is increased.

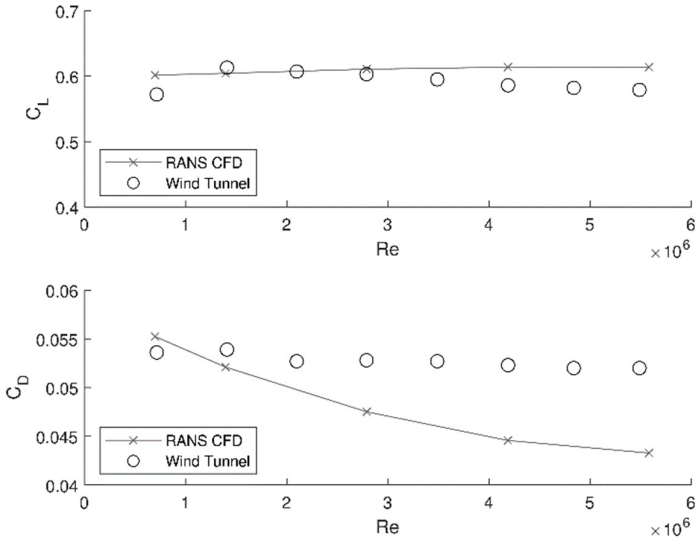

Figure 11. Comparison of the lift and drag coefficients from the wind tunnel experiment with RANS CFD simulation.

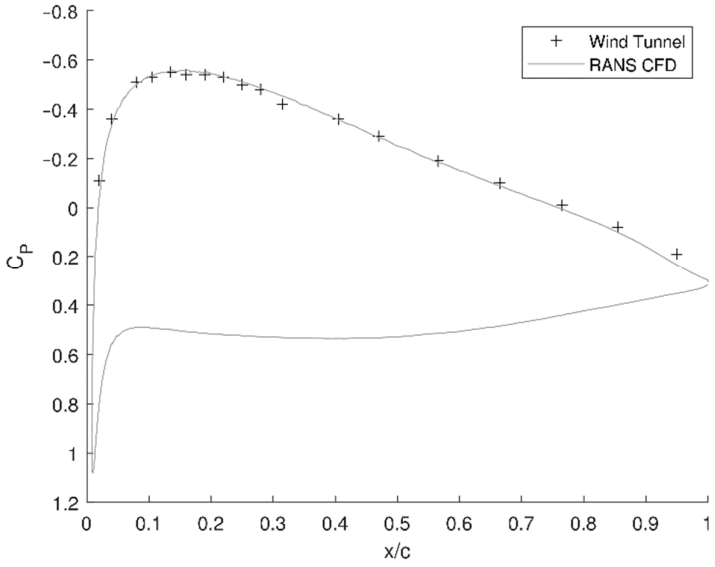

Figure 12. Comparison of the pressure distribution along half semi-span position stemming from current CFD simulation with the wind tunnel test results at 40 m/s.

In order to gain more insight into the qualitative behaviour of the flow around the AeroCity model, a particle trace image from the CFD model was compared with a fluorescent oil film photograph from the wind tunnel model. Note that the oil film pattern was obtained at a velocity U = 100 m/s, whereas the particle trace image from the CFD is made at U = 80 m/s. The two images are stacked together and shown in Figure 13. In order to enhance the visibility, the particle traces are coloured with the contour level of the local skin friction coefficient. Despite the small difference in free-stream velocity, the two surface trace patterns are relatively similar. It can be observed that the flow curls inboard after the location of maximum thickness as a result of the tip vortex. Since the local velocity is enhanced by the vortex, the skin friction coefficient in the area directly affected by

the vortex is larger than ambient. In both cases, it can also be observed that the trace lines are well organized and are parallel, indicating that the flow is attached to the surface. An exception is a zone near the trailing edge, in the case of the wind tunnel model. The local pattern of the oil film traces is an indication of the local separation of the flow.

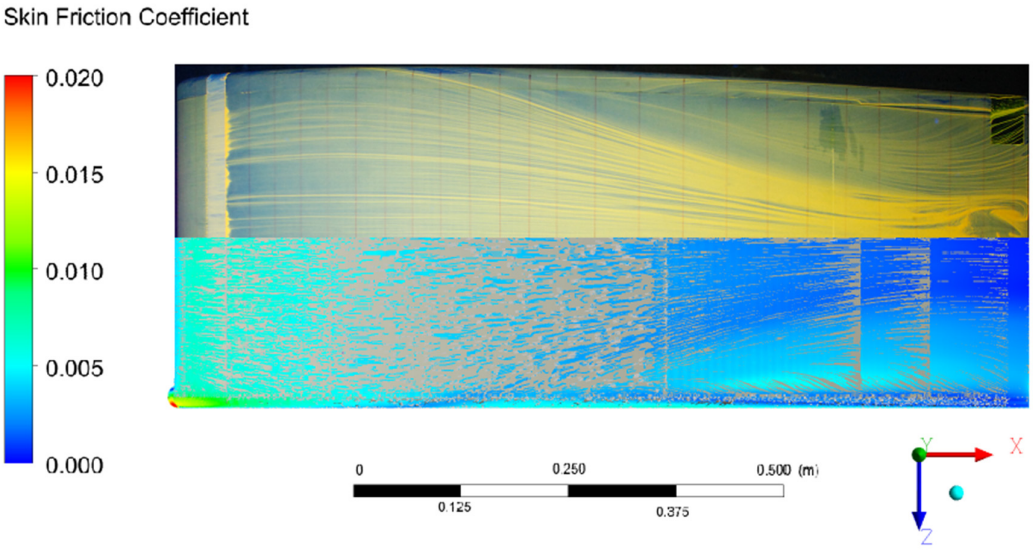

Figure 13. Comparison of upper surface fluorescent oil flow pattern obtained from the wind tunnel experiments (above) and particle image trace by CFD (below). Viewed from above, flow coming from the left.

A similar comparison is made for the flow around the side plates of the AeroCity model. This is presented in Figure 14. It can be seen that the general shape and size of the separation bubbles are different. In line with the previous observations, the separation bubble is much larger during the wind tunnel experiment. On the lower part of the side plate, the local flow pattern is significantly different. A strong upward flow component can be seen at the bottom of the front of the side plate. Although the resolution of the numerical particle trace is low in the zone directly after the leading edge, this strong upward flow component is not observed in the CFD result. As such, the lower separation bubble is predicted to be smaller than was recorded during the wind tunnel experiment.

To verify what contribution the separation bubble makes to the total drag generation of the AeroCity model, contours of the total pressure loss coefficient have been computed. As shown in Figure 15, the separation bubble appears to be one of the most prominent sources of drag. Aside from the separation bubble over the side plate, another source of total pressure loss that can be identified is the horseshoe vortex. In the vortex core, the losses are significant. Further downstream, the tip vortex, albeit smaller in size, also contributes to the loss of total pressure. Additionally, visible from the contour plot is the contribution of the boundary layer over the upper surface. In particular, near the trailing edge, where the displacement thickness of the boundary is the largest, the share to the drag of the AeroCity model is visible. What is also interesting in Figure 15 is the fact that the lower vortex can be seen to disperse in the lateral direction. The reason for this is the flow of air underneath the side plates. Due to the large pressure difference between both sides of the side plate, a portion of the lower side experiences high-pressure air 'leaks' from the exterior side of the side plate. Since the gap between the side plate and the ground plane is limited, the flow is accelerated. The 'jet-like' streams of air 'push' the lower vortex in the lateral direction. This principle was also observed by Nouwens [3] and

Park and Lee [22]. Both also reported the beneficial influence of the side plates on aerodynamic efficiency. The lateral displacement of the tip vortices may be one of the explanations for this, as the effective aspect ratio of the wing is increased when the vortices are displaced outboard. To gain more insight into the behaviour of the vortex structures, the vortices are visualized by means of the iso-surfaces of the Q-criterion [31]. The Q-criterion defines the vortex as a region where the vorticity magnitude is larger than the strain rate magnitude. Moreover, it requires the local pressure to be lower than ambient. The iso-surfaces of the values of the Q-criterion are presented in Figure 16. To enhance the comprehension of the vorticity and turbulent flow features, contours of the turbulent kinetic energy have been added to the iso-surfaces.

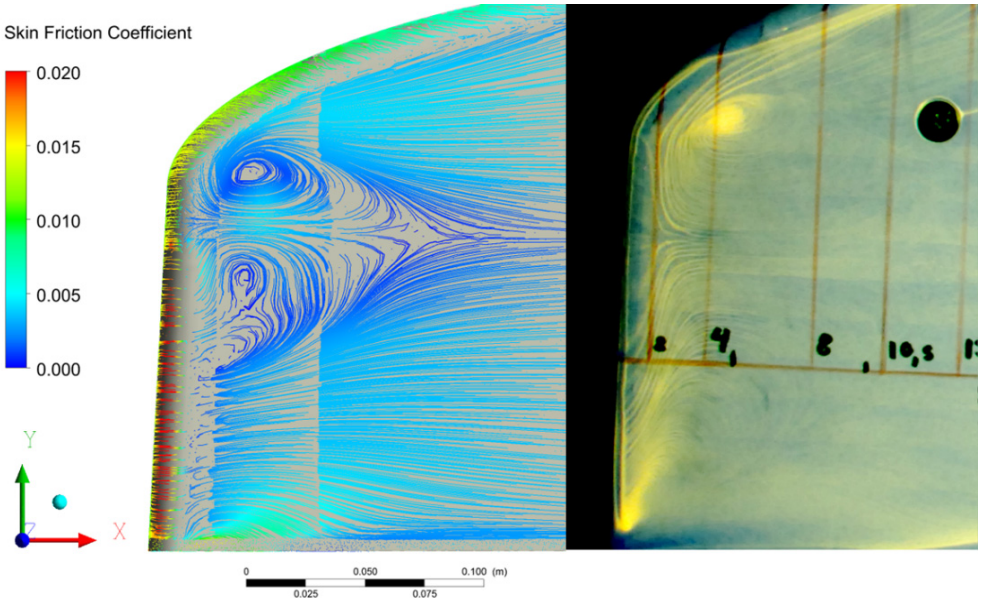

Figure 14. Comparison of side plate particle image trace by CFD (**left**) fluorescent oil flow pattern obtained from the wind tunnel experiment (**right**).

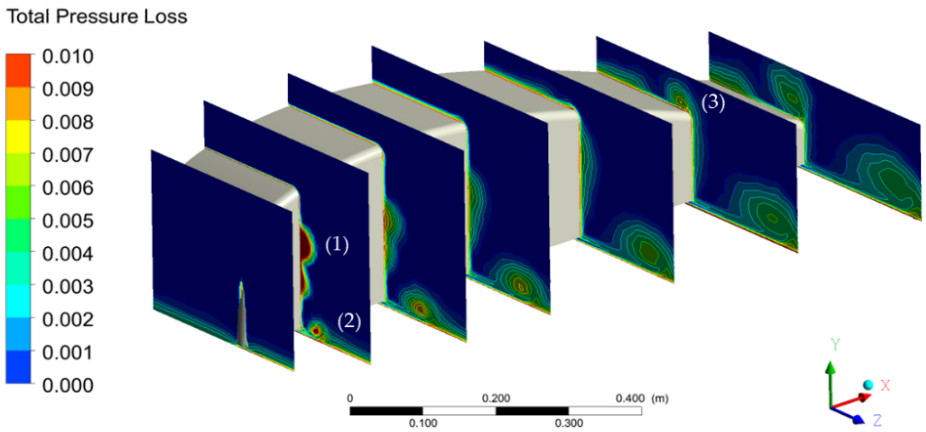

Figure 15. Contours of the total pressure loss coefficient at various chord-wise locations (U = 40 m/s). The laminar separation bubble (1), horseshoe vortex (2) and tip vortex (3) can clearly be identified.

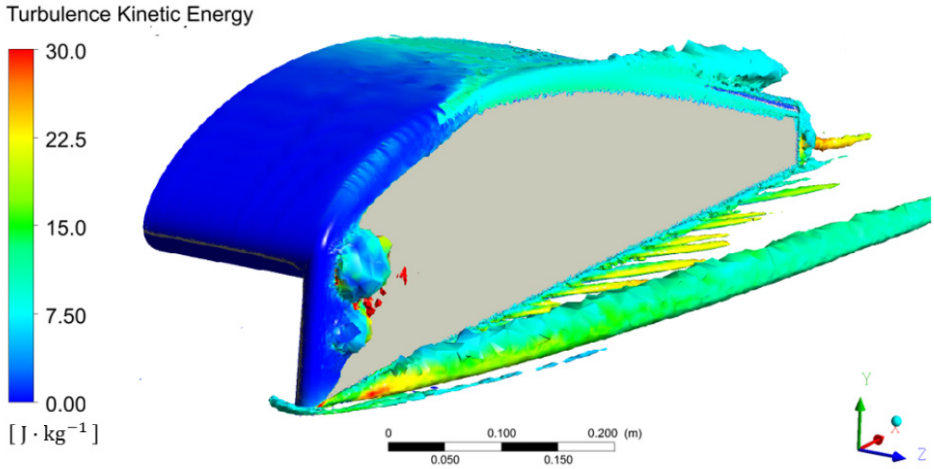

Figure 16. Iso-surface of Q-criterion (Q/Q_max = 0.001) and contours of the turbulence kinetic energy (U = 40 m/s).

The horseshoe vortex can be identified to be originating from the leading edge of the side plate. Aside from the lateral displacement of the vortex core, the iso-surface plot also shows that the vortex dissipates further downstream, beyond the trailing edge. The latter may be due to numerical dissipation in the CFD model. Furthermore, the intensity of the turbulent kinetic energy is found to be relatively high in the vortex core, still in close proximity to the vehicle. Another area of high turbulent kinetic energy is the area with the two separation bubbles over the side plate. Significantly, inside the centre of the separated flow region, the kinetic energy of the turbulent eddies is high. If the velocity of the free stream is increased, Figure 17 reveals that the size of the separation bubbles is reduced significantly, especially the lower bubble, which is almost absent at U = 80 m/s. The other flow features, such as horseshoe and tip vortices, appear to remain identical in terms of shape and size. Additionally, the contours of the turbulent kinetic energy (scaled with velocity) appear to be invariant of the free-stream velocity.

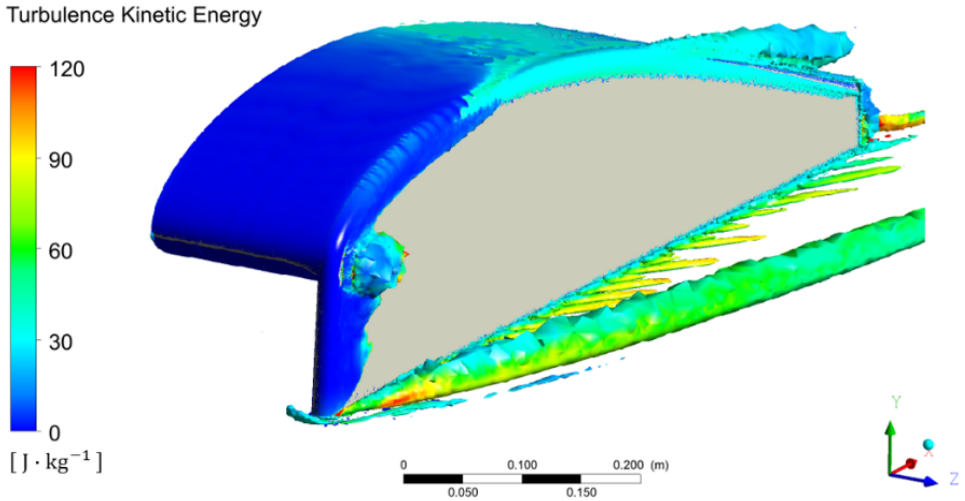

Figure 17. Iso-surface of Q-criterion (Q/Q_max = 0.001) and contours of the turbulence kinetic energy (U = 80 m/s).

To support the hypothesis that the under-prediction of the drag coefficient by the CFD model is caused by the under-prediction of the separation bubble size, the behaviour of the vehicle boundary layer was investigated. As observed in the fluorescent oil film photographs (Figure 13), some degree of flow separation near the trailing edge may have been present for the wind tunnel model. Since the particle traces obtained with CFD did not reveal any disturbances over the upper surface, a part of the deviation in drag coefficient may also stem from a difference in boundary layer development. As such, it is interesting to compare the boundary layer profiles of the experimental and numerical models.

The measurements of the boundary layer profiles were conducted at a free-stream velocity of U = 65 m/s. The upper surface of the AeroCity model was surveyed with a limited number of measurement locations along the symmetry plane. In total, the boundary layer profile was measured at five locations, distributed along the chord. The presented measurement of the boundary layer profiles is obtained with a fully turbulent boundary layer. Thus, with the trip location at $x/c = 0.05$, the boundary layer profiles were measured, as described previously, in terms of total pressure. However, to ease the comprehension of the data, the current results will be presented in terms of velocity. Using local measurements of the static pressure, the velocity distribution normal to the surface was recovered. Note that for the last measurement location ($x/c = 0.98$), the static pressure at $x/c = 0.95$ was used, since no data were available beyond this location. As such, there is a small offset in the data. Note that the total thickness of the prism layers in CFD was increased by two additional layers to bypass a spatial discretization error by the Fluent CFD software, which is related to the SST model parameters.

Taking the above limitations into consideration, the boundary layer profiles over the AeroCity upper surface were examined in more detail. Shown in Figures 18–21 are the velocity distributions from normal to surface, for both the experimental and numerical model. As can be seen, the results are in good agreement in the case of $x/c = 0.21$. Both the thickness and shape factor are similar. Further downstream, at $x/c = 0.46$, the agreement between the experimental findings and CFD predictions is still good, although a small difference in velocity magnitude can be observed. Continuing downstream, a growing discrepancy between both data sets is found. At $x/c = 0.65$, the shape factor of the boundary layer over the wind tunnel model is different compared to the computed boundary layer. Since the local pressure gradient is adverse, the shape factor of the boundary layer is increased. Apparently, this effect is not captured sufficiently well by the SST model, as the shape factor of the modelled boundary layer does not change. The difference between the experiments and the numerical model increases towards the trailing edge at $x/c = 0.98$. Here, the boundary layer over the wind tunnel model is on the verge of separation, whereas the CFD result remains well attached. Notice the small negative velocity component near the surface in the wind tunnel data. Although this may appear to indicate a local reversal of the flow, the negative values are in fact caused by the offset in static pressure, as discussed earlier. In terms of displacement thickness, the CFD model predicts a slightly larger overall thickness of the boundary layer.

Measuring and comparing the total pressure in the centre of the separation bubbles reveals that the size of the separation bubble was significantly larger than predicted by the CFD model. The peak of minimum total pressure is located approximately 30 mm in the normal direction to the surface of the side plate, whereas the local minimum in the case of the CFD model is located around 10 mm away from the side plate. Although the geometric location of both sample locations is different, these show that the separation bubble is not sufficiently captured by the CFD model.

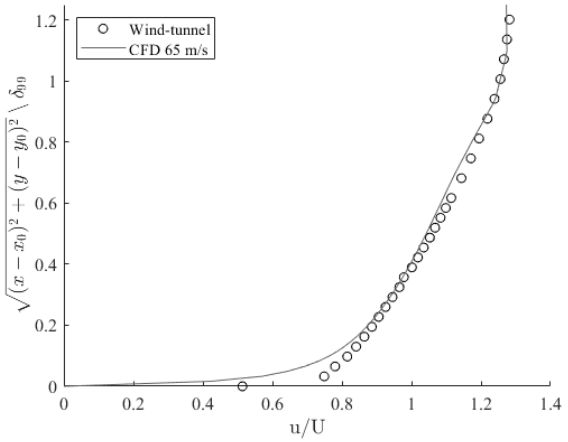

Figure 18. Measurement of velocity profile normal to the surface at x/c = 0.21. Comparison between CFD and experimental data.

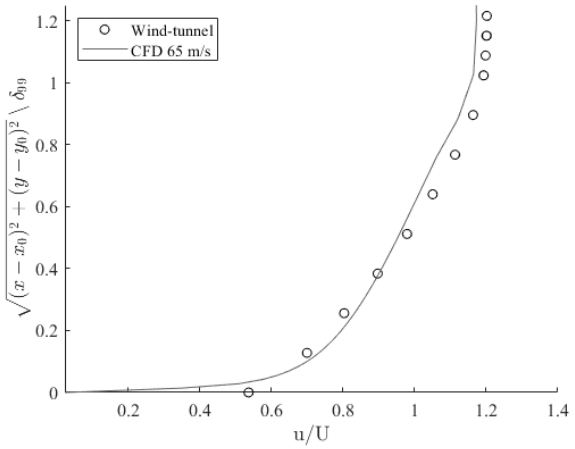

Figure 19. Measurement of velocity profile normal to the surface at x/c = 0.46. Comparison between CFD and experimental data.

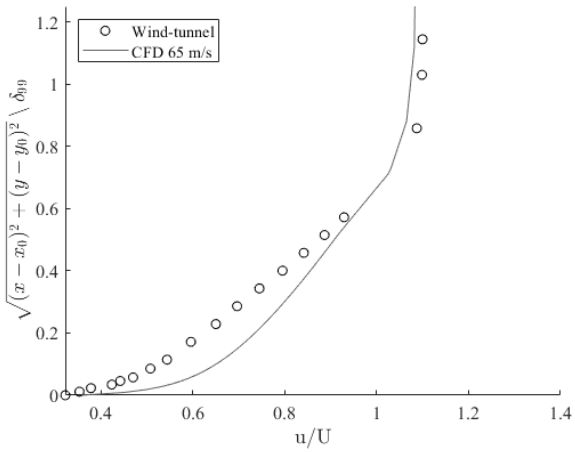

Figure 20. Measurement of velocity profile normal to the surface at x/c =0.65. Comparison between CFD and experimental data.

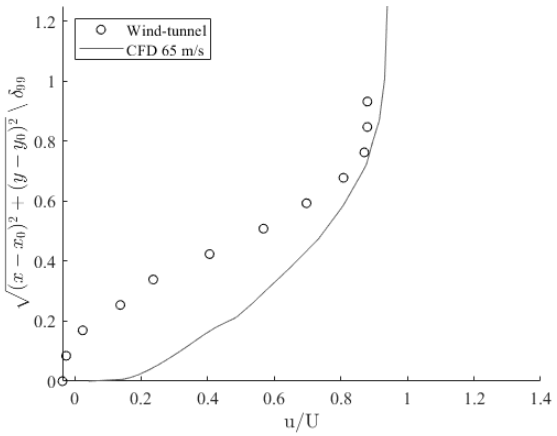

Figure 21. Measurement of velocity profile normal to the surface at x/c = 0.98. Comparison between CFD and experimental data.

4.5. Transition Model

During the wind tunnel experiment, the laminar flow was tripped at the location of x/c = 0.05 by means of two layers of dual-sided tape. However, this was only applied to the upper surface. Hence, the flow over the leading edge of the side plate may have been laminar depending on the diameter-based Reynolds number. The computation of the latter shows that the Reynolds number varied between Re_d = 1.7 × 10^4 and Re_d = 1.4 × 10^5. Middleton and Southard [32] showed that the location of flow separation on a cylinder shifts downstream with an increase in the $\mathrm{Re_d}$. Hence, the size of the wake is dependent on the local Reynolds number. In general, it is found that the boundary layer over a cylinder transitions from laminar to turbulent at around $\mathrm{Re_d}$ ≈ 4 × 10^5. Assuming a relatively low surface roughness, it can be assumed that the flow over the leading edge of the side plate was laminar during the wind tunnel experiment. However, the flow was fully turbulent in the CFD model. As the wake behind a cylinder subjected to a flow past the critical Reynolds number is significantly smaller, the drag characteristics are different. In fact, the drag coefficient for a cylinder in super-critical flow is C_D ≈ 0.30, while a cylinder in a sub-critical flow features a drag coefficient of C_D ≈ 1.20. Although the drag of the AeroCity consists of other contributors, such as drag due to the generation of vortices, it is clear that the simulation of the flow around the AeroCity model in a fully turbulent domain may be one of the primary causes for the under-prediction of the drag by the CFD model.

In order to improve the predictions by the CFD model, the implementation of a transitional turbulence model (Transition SST model) was investigated. The scenario with the stationary ground, resembling the exact wind tunnel conditions, was simulated. The results show that the drag force prediction with the transition turbulence model was lower compared to the results obtained with the fully turbulent flow assumption (ΔC_D = −0.0030). However, if one examines the sources of the drag coefficient, one finds that the pressure drag is increased by more than ΔC_D = 0.0330. In contrast, the skin friction drag is reduced by ΔC_D = −0.0370. The increase in the pressure drag indicates that the separation bubble may have been improved. A direct comparison of the particle surface traces from the simulation and the fluorescent oil film photograph of the experiment, shown in Figure 22, clearly shows that the size of the separation bubble is significantly increased compared to the previous result. Significantly, the flow over the lower part of the side plate appears to be captured to a better extent. Since the separation bubble is directly dependent on the Reynolds number, a separation bubble is not expected to be present for the full-scale AeroCity model. Nevertheless, in order to validate the CFD simulations with experimental data, the structure and means to reduce the separation bubble should be further investigated. From the work of Chong and Perry [33], it can be seen that the flow

pattern resembles that of a fifth-order unsymmetrical owl face of the first kind. Chong and Perry studied the patterns of separated flows, including the separation bubbles and the origin of vortices, using the analysis of critical points. By locally expanding the Navier–Stokes and continuity equations by means of a Taylor series expansion around a set of critical points, the local three-dimensional streamlines can be derived. To further study the structure and the behaviour of the separation bubble, the Critical Point Theory [34] could be very useful.

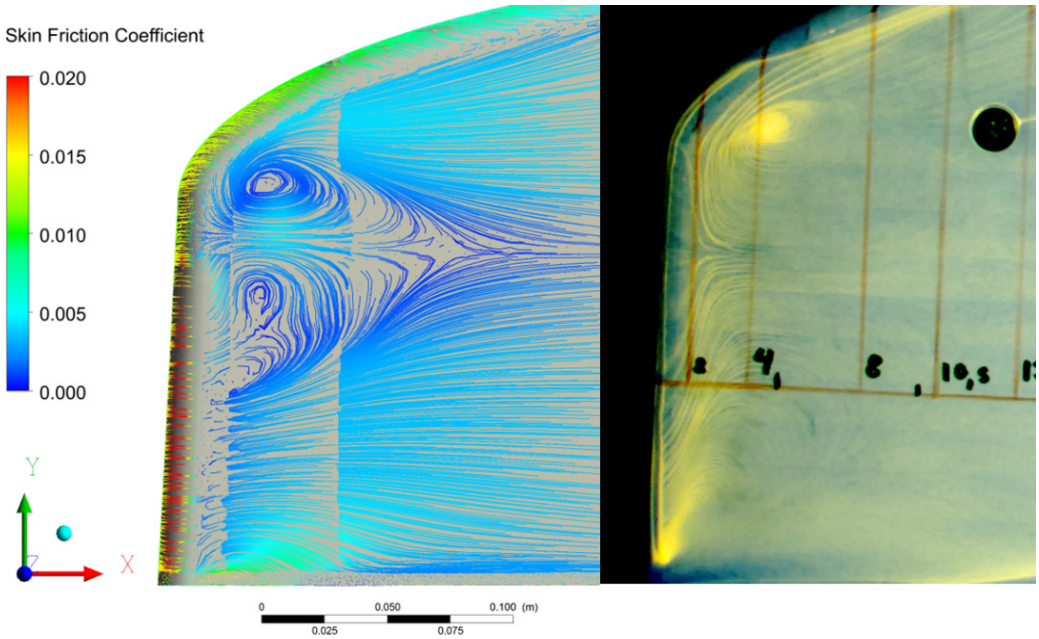

Figure 22. Comparison of fluorescent oil film from the wind tunnel experiment and surface particle traces obtained with the Transition SST turbulence model.

4.6. Moving Ground

Although there is a discrepancy between the results obtained from the wind tunnel and the CFD model, the effect of the moving ground boundary condition can easily be modelled numerically. Since, according to the literature [10,11], a moving ground boundary condition is preferred, the wall boundary condition in the CFD model was adapted to the free-stream velocity.

In terms of force coefficients, the difference between the two boundary conditions is within the error margin, with an increase in the aerodynamic efficiency of less than 2%. The investigation of the C_p distribution shows that the pressure distribution is almost identical. The C_p values are slightly more negative over the upper and lower surface in the case of the moving ground boundary condition. This indicates a shift in the location of the stagnation point. Shown in Figure 23 is the velocity profile over the flow channel between the AeroCity model and the ground plane. The difference in the velocity gradient near the ground is significant. The displacement thickness of the boundary layer over the ground plane is equal to almost 30% of the height of the flow channel. As a result, the effective flow channel is reduced by the presence of the ground boundary layer. Over the entire flow channel, the velocity is, therefore, lower in the case of the moving ground boundary condition.

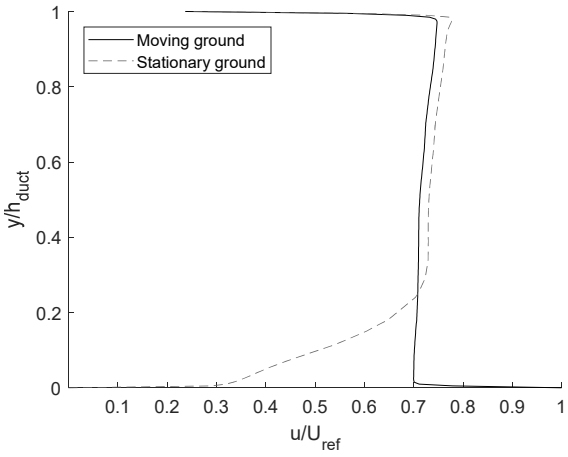

Figure 23. Non-dimensional velocity profile of the flow channel between the AeroCity and the ground plane at x/c = 0.10 and U = 40 m/s.

An explanation for the insignificant effect of the ground boundary condition on the aerodynamics of the AeroCity model may be found in the work of Fliag [35]. According to the findings of Fliag, a lifting surface can only be considered to be in ground effect if the ratio between the lift coefficient and the elevation height over span (h/b) exceeds at least 20. However, the average lift coefficient at which the wind tunnel model was operating is below $C_L = 0.60$. Due to the low aspect ratio of the AeroCity model, the height-over-span ratio is only h\b=0.125. Therefore, the wind tunnel model was operating outside the bounds for which the ground modelling is of importance, according to Fliag. Decreasing the height-over-chord ratio and increasing the lift coefficient would be required to experimentally investigate the IGE behaviour of the AeroCity, assuming that the aspect ratio is not altered.

4.7. Inclusion of a Track Wall

One important aspect of the AeroCity concept is the fact that it is envisioned to operate inside a track. Ideally, the track should not only provide lateral guidance, but also enhance the WIG effect. In theory, the side walls of the track could help to suppress the formation of the lower tip vortices and maintain the 'cushion' of high-pressure air underneath the vehicle. However, the effect of a track wall on the aerodynamics of a WIG vehicle has not been investigated. Since the design of the track for AeroCity is still uncertain at this point, a generic U shape has been assumed. Assuming a full-scale model, a wall height of 1.00 m was selected, as well as a lateral gap between the vehicle and the wall of 0.30 m. Note that for the analysis, the same model scale (1:20) was used, and the track was scaled accordingly. A schematic drawing of the conceptual track design is shown in Figure 24.

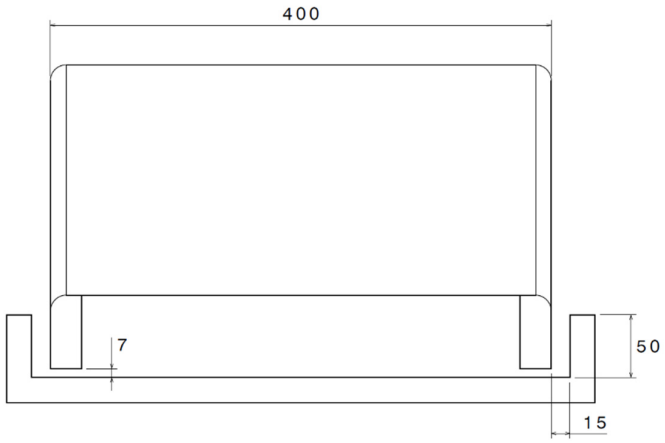

Figure 24. Drawing of the track design from the rear side of the wind tunnel model. Dimensions in millimetres, wind tunnel model scale (1:20).

The wall was modelled with a no-slip boundary condition with an absolute velocity equal to the free stream. From the initial analysis, it is found that the presence of the track wall has a significant impact on the aerodynamic performance of the AeroCity model. Shown in Table 5 are the force coefficients for both the cases, i.e., in the presence and absence of the track side wall. As can be observed, the lift was, indeed, marginally increased by the addition of a track wall. However, the effect is modest and is within the range of the numerical errors. The drag coefficient on the other hand is found to be increased by a significant amount. As such, there is a net decrease in the aerodynamic efficiency of the AeroCity model by around 6%. Hence, at least for the current track geometry, the track appears to have a detrimental effect on the aerodynamics of the vehicle. An investigation of the pressure distribution, at half span, reveals that over the aft upper surface, the C_p values are lower than the case without a track. This suggests that the influence of the tip vortices has become more pronounced. A comparison of the Q-criterion surfaces, shown in Figure 25, reveals that the lower tip vortex is not suppressed by the track wall, but rather deflected upwards. Halfway downstream, the lower vortex merges with the upper tip vortex into a single strong vortex. This partially explains the increased drag levels, as the skin friction is enhanced in the regions surrounding the vortex. The single tip vortex is also responsible for the minor increase in the lift, as suction is enhanced over the aft upper surface. Due to the additional upward flow component, the separation bubble can be seen to have grown in size. Moreover, only a single bubble appears to be in existence. An additional effect of the track wall is that the 'leaked flow' is also deflected upwards and partially trapped between the wall and the vehicle. Due to the large velocity gradient over the lateral gap, the flow becomes highly turbulent. As such, the frictional losses are considerable and translates into an increase in momentum drag. Downstream of the trailing edge, the 'jet-like' flow of highly turbulent air curls into a separate vortex, causing additional pressure drag. Although only a single non-optimized track design has been investigated, this shows that the influence of the track on the aerodynamics of the vehicle can be significant.

Table 5. Comparison of force coefficients for the case with and without a track wall present for U = 40 m/s. Force coefficients.

Case	C_L	C_D	L/D
Moving ground, no track	0.6122	0.04707	13.0
Moving ground, with track	0.6170	0.05075	12.2
	+0.8%	+7.8%	−6.5%

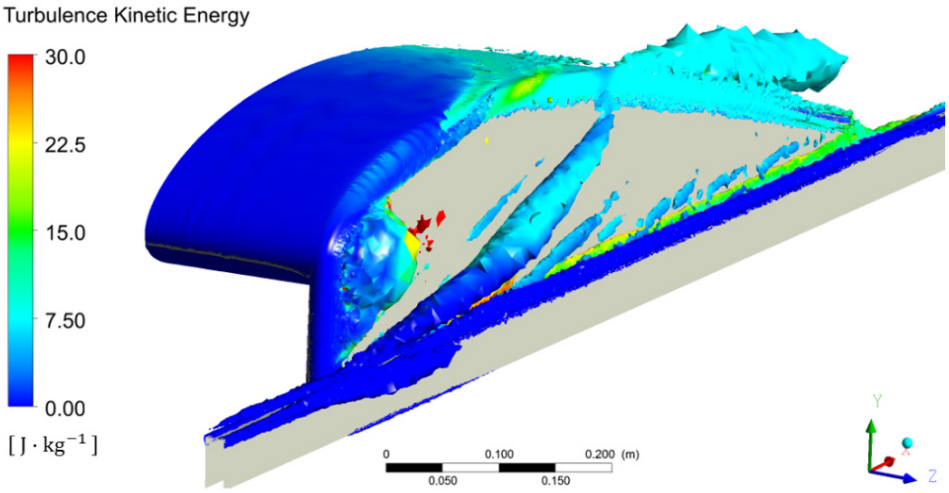

Figure 25. Iso-surface of Q-criterion (Q/Q_max = 0.001) and contours of the turbulence kinetic energy with a track wall (U = 40 m/s).

5. Conclusions

To summarize the current work, it can be concluded that the basic aerodynamic characteristics of the AeroCity model have been successfully investigated. The wind tunnel experiment explored the sensitivity of the aerodynamic performance indicators to the main design parameters. Despite a few limitations (e.g., a stationary wall), the results of the wind tunnel experiment showed that the basic aerodynamic configuration of the AeroCity model is feasible. The main discovery of the experiment is the existence of two separation bubbles over the side plates of the scaled vehicle. Subsequent CFD modelling of the same aerodynamic model was performed to further analyse the aerodynamic characteristics of the AeroCity model and explore the ability of the CFD models to replicate the experimental conditions.

Prior to the simulation of the AeroCity model, a validation study of a comparative WIG effect study [30] was performed. The comparison showed that the CFD model was able to successfully predict the main aerodynamic characteristics of the ground-effect vehicle. Nevertheless, a deviation in the drag force prediction of about 10% was found regardless of the selected turbulence model.

The main analysis of the AeroCity model revealed that the CFD model and the wind tunnel measurements are in reasonable agreement. In general, the boundary layer profiles matched to a good extent. Only towards the trailing edge, the numerically computed boundary layer profiles remained insensitive to the local adverse pressure gradient. As such, the small zone of flow separation near the trailing edge, as observed during the wind tunnel experiment, was not captured by the CFD model. Furthermore, the separation bubbles over the side plates appeared to be under-predicted. A comparison of the fluorescent oil film photographs and surface particle traces from CFD revealed that the size of the separation bubbles in the numerical results is, indeed, significantly smaller than as observed during the experiment. These two effects together resulted in a growing error in the prediction of the CFD model for the drag coefficient. The use of a transition turbulence model significantly improved the prediction of the separation bubble. Nevertheless, due to a delayed onset of the transition of the flow from laminar to turbulent, the inclusion of a transition model did not improve the overall prediction of the drag coefficient. The prediction of the separation bubble by the CFD models is important in order to validate the CFD results with experimental data, even though no large separation bubbles are expected at this location in the full-scale model. The formation of a separation bubble on the

scaled model may be avoided by reshaping the leading edge of the side plates or adding transition strips to ensure turbulent flow over the side plates.

Furthermore, the addition of a moving ground plane and a track wall have been investigated for the AeroCity model. Based on reports available in the literature [10,11,22], the influence of the ground boundary condition on the aerodynamic performance of the WIG vehicle is significant. However, the current numerical results suggest that this may not be true in all cases. Switching to a moving ground boundary condition did not have a significant effect on the aerodynamics of the AeroCity model. However, reviewing further literature [35] revealed that the ratio of the wing lift coefficient and elevation height over span of the AeroCity model is too low to consider the ground boundary condition. As such, a further reduction in the elevation height or an increase in the span or lift coefficient is required to make use of the extreme ground effect. Regarding the track wall, the analysis has shown that the inclusion of a U-shaped track wall has a negative effect on the aerodynamic performance of the AeroCity model. Although only a single-track design has been tested and many parameters can be varied, the simulation shows that the track has an important role in the aerodynamic behaviour of the vehicle. As such, the vehicle and track should not be designed separately, but rather developed synergistically. A different track design, such as the V-shaped track design proposed by Nouwens [3], or an inboard track design, may provide an alternative to the current track geometry.

Although the basic aerodynamic configuration of the AeroCity model appears to be feasible, further study is required to investigate more details about the aerodynamics of this unique configuration. Significantly, the topic of the dynamic longitudinal stability of the AeroCity needs further research to address questions about passenger safety and comfort.

Author Contributions: Conceptualization: A.G.R.; Methodology: S.N.; Validation: G.E.; Formal analysis: M.v.S.; Investigation: M.v.S., S.N.; Resources: A.G.R.; Writing original draft: M.v.S.; Writing review and editing: M.v.S., A.G.R., G.E.; Supervision: A.G.R., G.E. All authors have read and agreed to the published version of the manuscript.

Funding: This research received no external funding.

Acknowledgment: The authors would like to thank Everard van Rees, the inventor of the AeroCity concept, for sharing his ideas with us. The authors would also like to thank Mark Voskuijl, faculty of Military Sciences at the Netherlands Defence Academy, and Leo Veldhuis for their help and advice with the wind tunnel testing.

Conflicts of Interest: The authors declare no conflict of interest.

References

1. Ollivier, G.; Sondhi, J.; Zhou, N. *High-Speed Railways in China: A Look at Construction Cost, China Transport Topics*, 9th ed.; The World Bank: Beijing,China, 2014.
2. Movares, B.V. Available online: https://www.railcenter.nl/wp-content/uploads/2017/02/02-Innorail-Inspiratie-ideeen-2017-Everard-van-Rees-v01.pdf (accessed on 7 June 2019).
3. Nouwens, A.T. Aerodynamic Performance and Stability Analysis of AeroCity. Master's Thesis, Delft University of Technology, Delft, The Netherlands, March 2011.
4. Ahmed, M.R.; Sharma, S.D. Experimental Investigation of the Flow Field of a Symmetrical Airfoil in Ground Effect. In Proceedings of the 21st Applied Aerodynamics Conference, Orlando, FL, USA, 23–26 June 2003.
5. Ahmed, M.R. Aerodynamics over Thick Airfoils in Ground Effect–An Investigation on the Influence of Camber. In Proceedings of the 24th Congress of International Council of the Aeronautical Sciences, Yokohama, Japan, 29 August–3 September 2004; pp. 1–11.
6. Ahmed, M.R. Aerodynamics of a NACA 4412 Airfoil in Ground Effect. *AIAA* **2007**, *45*, 37–47.
7. Ahmed, M.R. Aerodynamics of a Chambered Airfoil in Ground Effect. *Int. J. Fluid Mech.* **2005**, *32*, 157–183.
8. Hsiun, C.M.; Chen, C.K. Aerodynamic Characteristics of a Two-Dimensional Airfoil with Ground Effect. *J. Aircr.* **1996**, *33*, 386–392.
9. ZYang, G.; Yang, W.; Jia, Q. Ground Viscous Effect on 2D Flow Wing in Ground Proximity. *Eng. Appl. Comput. Fluid Dyn.* **2010**, *4*, 521–531.

10. George, A.R. Aerodynamic Effect of Shape, Camber, Pitch and Ground Proximity on Idealized Ground-Vehicle Bodies. *J. Fluids Eng.* **1981**, *103*, 631–637
11. Barber, T.J. Aerodynamic Ground Effect: A Case Study of the Integration of CFD and Experiment. *Int. J. Veh. Des.* **2006**, *40*, 299–316.
12. Ockfen, A.E.; Matveev, K. Aerodynamic Characteristics of NACA 4412 Airfoil Section with Flap. *Int. J. Nav. Archit. Ocean Eng.* **2009**, *1*, 1–12.
13. Hase, S.; Eitelberg, G.; Veldhuis, L. Ground Effect Investigation for Two Dimensional Airfoil. In Proceedings of the Symposium on Experiments and Simualtion of Aircraft in Ground Proximity, Germand-Dutch Wind Tunnels DNW, Marknesse, The Netherlands, April 2013.
14. Gross, J.; Traub, L.W. Experimental and Theoretical Investigation of Ground Effect at Low Reynolds Numbers. *J. Aircr.* **2012**, *49*, 576–586.
15. Wieselberger, C. Wing Resistance near the Ground, Zeitschrift fur Flugtecknik und Motorluftshiffart. *Z. Flugtecknik Mot.* **1922**, *10*, 145–147.
16. Prandtl, L. Tragflügeltheorie, Nachrichten von der Gesellschaft der Wissenschaften zu Göttingen. *Math.-Phys. Kl. 1918* **1918**, *285–288*, 451–477.
17. Betz, A. Lift and Drag of a Wing near a Horizontal Surface (the Ground). *Z. Flugtecknik Mot.* **1912**, *3*, 217.
18. Philips, W.E.; Hunsaker, D.E. Lifting-line Predictions for Induced Drag and Lift in Ground Effect. *J. Aircr.* **2013**, *50*, 1226–1233.
19. Traub, L.W. Experimental and Analytic investigation of Ground Effect. *J. Aircr.* **2014**, *52*, 235–234.
20. Fink, M.P.; Lastinger, J.L. *Aerodynamic Characteristics of Low-Aspect Ratio Wings in Close Proximity to the Ground*; National Aeronautics and Space Administration: Washington, DC, USA, 1961.
21. Chawla, M.D.; Edwards, L.C.; Franke, M.E. Windtunnel Investigation of Wing-in-Ground Effects. *J. Aircr.* **1990**, *27*, 289–293.
22. Park, K.; Lee, J. Influence of Side-plate on Aerodynamic Characteristics of Low-Aspect-Ratio Wing in Ground Effect. *J. Mech. Sci. Technol.* **2008**, *22*, 2578–2589.
23. Jung, J.H.; Kim, M.J.; Yoon, H.S.; Hung, P.A.; Chun, H.H.; Park, D.W. Endplate Effect on Aerodynamic Characteristics of Three-Dimensional Wings in Close Free Surface Proximity. *Int. J. Nav. Archit. Ocean Eng.* **2012**, *4*, 477–487.
24. Cho, J.; Han, C. Unsteady Trailing Vortex Evolution behind a Wing in Ground effect. *J. Aircr.* **2005**, *42*, 429–434.
25. Krasny, R. Computation of Vortex Sheet Roll-Up in the Trefftz Plane. *J. Fluid Mech.* **1987**, *184*, 123–155.
26. Lee, J.; Han, C.S.; Bae, C.H. Influence of Wing Configurations on Aerodynamic Characteristics of Wings in Ground Effect. *J. Aircr.* **2010**, *4*, 1030–1040.
27. Patankar, S.V.; Spalding, D.B. A Calculation Procedure for Heat, Mass and Momentum Transfer in Three-Dimensional Parabolic Flows. *Int. J. Heat Mass Transf.* **1972**, *10*, 1787–1806.
28. van Leer, B. Towards the Ultimate Consevative Difference Scheme V–A Second-Order Sequal to Gundov's Method. *J. Comput. Phys.* **1979**, *32*, 101–136.
29. Leonard, B.P. A Stable and Accurate Convective Modeling Procedure based on Quadratic Upstream Interpolation. *Comput. Methods Appl. Mech. Eng.* **1979**, *19*, 59–98.
30. Kumar, P.E. An Experimental Investigation into the Aerodynamic Characteristics of a Wing with and with-out Side-plates. In *College of Aeronautics Report Aero No. 201*; College of Aeronautics Cranfield: Bedfordshire, UK, 1968.
31. Hunt, J.C.R.; Wray, A.A.; Moin, P. Eddies, Streams and Convergence Zones in Turbulent Flows. In *Proceedings of the Summer Program, 89*; Centre for Turbulence Research: Stanford, CA, USA, 1988
32. Middleton, G.V.; Southard, J.B. *Mechanics of Sediment Movement*, 2nd ed.; Society of Economic Paleontologists and Mineralogist: Tulsa, OK, USA, 1984.
33. Chong, M.S.; Perry, A.E. Synthesis of Two and Three-dimensional Separation Bubbles. In Proceedings of the 9th Australian Fluid Mechanics Conference Auckland, Auckland, New Zealand, 8–12 December 1986.
34. Perry, A.E.; Fairlie, B.D. Critical Points in Flow Patterns. *Adv. Geophys.* **1975**, *18 Pt B*, 299–315.
35. Flaig, A. Results of wind tunnel ground effect measurements on Airbus A320 using turbine power simulation and moving tunnel floor techniques. In Proceedings of the 16th Aerodynamic Ground Testing Conference, Seattle, WA, USA, 18–20 June 1990.